

Low T cell receptor expression and thermal fluctuations contribute to formation of dynamic multifocal synapses in thymocytes

Sung-Joo E. Lee^{**†}, Yuko Hori^{†§¶||}, and Arup K. Chakraborty^{*†§¶***††}

Departments of ^{**}Chemical Engineering, [§]Chemistry, and ^{||}Physics and ^{*}Biophysics Graduate Group, University of California, Berkeley, CA 94720; and [†]Materials Science Division and [¶]Physical Biosciences Division, Lawrence Berkeley National Laboratory, Berkeley, CA 94720

Communicated by David Chandler, University of California, Berkeley, CA, January 29, 2003 (received for review September 20, 2002)

Mature T cell activation and selection of immature T cells (thymocytes) are both initiated by binding of T cell receptor (TCR) molecules on the surface of T cells to MHC peptide (MHCp) molecules on the surface of antigen-presenting cells. Recent experiments have shown that the spatial pattern of receptors and ligands in the intercellular junction (synapse) is different during thymocyte selection compared with mature T cell activation. Using a statistical mechanical model, we show that lower TCR expression in thymocytes contributes to effecting these differences. An analogy with the phase behavior of simple fluids helps clarify how, for low TCR expression, thermal fluctuations lead to the dynamic synapse patterns observed for thymocytes. We suggest that a different synapse pattern resulting from lower TCR expression, which could mediate differential signaling, may be the reason why TCR expression level is low in thymocytes.

Activation of mature T lymphocytes (T cells) in response to pathogens and the maturation and selection of immature T cells (thymocytes) in the thymus leading to the available T cell repertoire are key features of an adaptive immune system (1). Antigen-presenting cells (APCs) catabolize pathogen-derived protein into small peptide fragments. These peptides can bind to proteins coded for by the major histocompatibility gene, and the resulting complexes [MHC peptide (MHCp)] are then displayed on the APC surface. Binding of T cell receptor (TCR) molecules expressed on the T cell surface to these MHCp complexes initiates intracellular signaling cascades that can activate mature T cells (2), resulting in effector functions such as cytokine production, proliferation, and killing of target cells (3, 4).

Recent *in vitro* and *in vivo* experiments have demonstrated that during mature T cell activation different types of receptors and ligands segregate to different regions of the T cell–APC junction (5–13). The resulting spatial pattern of receptors and ligands is called the immunological synapse. A temporally stable mature immunological synapse forms in many minutes and is characterized (Fig. 1*a*) by a central accumulation of TCR and MHCp (cSMAC) and a peripheral ring of adhesion molecules (pSMAC). A number of recent studies have provided partial answers to the question of how the synapse forms (5–19), but its role in T cell activation is not well understood.

Thymocyte selection and maturation in the thymus also requires binding of TCR to MHCp complexes displayed on thymic APCs (20). The peptides in this case are derived from proteins characteristic of the organism (self-peptides). Thymocytes undergo either positive or negative selection after TCR–MHCp binding (20–24). Positive selection is a step toward the development of mature T cells, whereas negative selection corresponds to apoptosis triggered by strong TCR–MHCp binding. Some details of signaling during thymocyte development and mature T cell activation are different (25). However, because most of the initial molecular players and signaling pathways involved in mature T cell activation and thymocyte selection are the same, an important question emerges: Why are the biological consequences of similar signaling cascades initiated by TCR–MHCp binding different in the two cases? This question has motivated recent experiments (26–28) that examine

whether synapse patterns at thymocyte–APC junctions are different from those observed during mature T cell activation.

In vitro experiments have been carried out with CD4⁺CD8⁺ double-positive (DP) thymocytes interacting with thymic stromal cells (27) and with supported bilayer mimics of thymic APCs (26). There are some differences between the synapse patterns observed in these two kinds of experiments. However, common features are that there is no central accumulation of TCR and that the synapse pattern is dynamic, in contrast to the stable cSMAC observed during mature T cell activation (Fig. 1).

TCR expression levels are substantially lower in DP thymocytes compared with mature T cells (26, 29–31). We use a statistical mechanical model to study whether this difference in TCR expression level underlies disparities between the synaptic patterns formed during thymocyte selection and that observed during mature T cell activation. We find that low TCR expression prevents the formation of a well organized synapse, and thermal fluctuations contribute to the formation of dynamic synapse patterns observed in experiments with DP thymocytes. We describe the forces that lead to multifocal dynamic synapses in terms of an analogy with the phase behavior of a simple fluid. In this analogy, TCR expression level determines the system free energy in much the same way as temperature determines the dependence of free energy on molar volume in a simple fluid.

Recent Experiments and Choice of Model

Richie *et al.* (27) studied conjugates between 5C.C7 DP thymocytes (from transgenic mice) and thymic stromal cells in an environment that simulates the three-dimensional *in vivo* environment of lymphoid organs. They found that, when the functional outcome is negative selection, CD3 (TCR) largely accumulates in the periphery of the synapse. The accumulation pattern is dynamic, however, and boluses of CD3 form, disappear, and reappear in the central region of the synapse.

Hailman *et al.* (26) imaged thymocytes interacting with a planar bilayer containing MHCp and intercellular adhesion molecule 1 (ICAM-1). They found that DP thymocytes form synapses that are multifocal and dynamic (Fig. 1*b*). Small clusters of MHCp are seen in a background of ICAM-1 in the intercellular junction. As in experiments with stromal cells (27), the synapse is dynamic, and MHCp clusters form in particular spots, evanesce, and reappear in different parts of the junction (26).

There are many possible reasons for the stark contrast between dynamic synapses formed by thymocytes and stable synapses characteristic of mature T cells. Examples include the lack of costimulatory molecules such as B7 on thymic APCs and differences in membrane characteristics between thymic APCs and those involved in mature T cell activation. Experiments with supported

Abbreviations: APC, antigen-presenting cell; MHCp, MHC peptide; TCR, T cell receptor; DP, double-positive; ICAM-1, intercellular adhesion molecule 1; LFA-1, lymphocyte function-associated antigen 1.

[§]S.-J.E.L. and Y.H. contributed equally to this work.

^{††}To whom correspondence should be addressed. E-mail: arup@uclink.berkeley.edu.

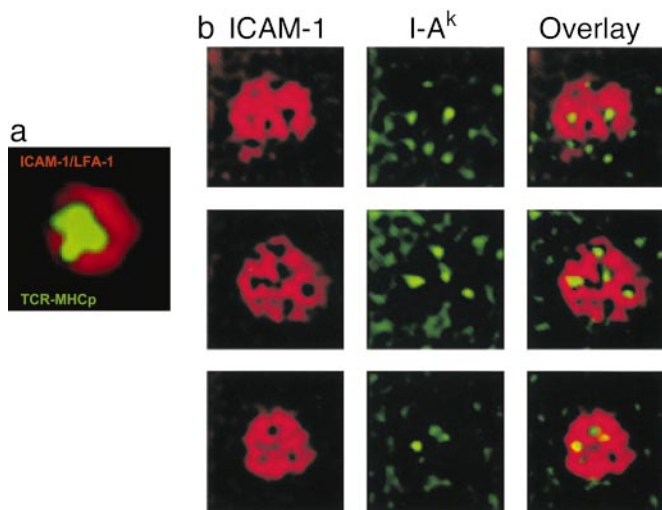


Fig. 1. (a) Fluorescent video-microscopy image of the stable synapse formed at the intercellular junction between mature T cells and supported bilayers containing ICAM-1 and MHCp. The image is taken looking down from the top of the T cell at the intercellular junction. The spatial distribution of MHCp (green) and ICAM-1 (red) is shown (5). Once formed, this pattern is stable for >30 min. (b) Fluorescent video-microscopy images of synapse formation at the intercellular junction between DP thymocytes and supported bilayers containing ICAM-1 and MHCp (26). All images are looking down from the top of the thymocyte at the intercellular junction. The three rows correspond to three different time points spaced 2 min apart. In the overlay, green corresponds to MHCp and red corresponds to ICAM-1. The synapses are $\approx 10 \mu\text{m}$.

bilayers, however, do not incorporate these physiologically important differences between different types of APCs, and these factors cannot underlie the observations by Hailman *et al.* (26).

A supported bilayer containing only ICAM-1 and MHCp represents a common controlled substrate with which both mature T cells and thymocytes can interact. Therefore, although less realistic than experiments with cell–cell conjugates, experiments with supported bilayers provide an opportunity to examine whether certain characteristics inherent to the stage of T cell maturity contribute to the dynamic character of thymocyte synapse patterns with bilayers and thymic stromal cells. It should be noted that most qualitative observations regarding synapse formation using the bilayer experimental platform and living APCs are consistent with each other (5–8, 11, 13, 26, 27). In the rest of this article, we focus on the supported bilayer experimental platform. However, insights that we obtain are connected to observations reported for cell–cell aggregates (27, 28).

DP thymocytes from transgenic mice used by Hailman *et al.* (26) have a TCR expression level that is significantly (at least 1 order of magnitude) smaller than mature T cell controls. Richie *et al.* (27) also used thymocytes from transgenics that have a lower level of TCR expression (M. M. Davis, private communication). *In vivo*, nontransgenic DP thymocytes express low levels of TCR, and the expression level increases as cells mature in the thymus. This leads us to investigate whether the inherently low TCR expression can lead to dynamic synapse patterns for DP thymocytes. The expression of lymphocyte function-associated antigen 1 (LFA-1) on the transgenic thymocytes used in the experiments by Hailman *et al.* (26) is also somewhat smaller than in mature T cells. However, the decrease is modest compared with the large change in TCR expression levels, and thus we kept the LFA-1 expression level constant in our studies.

Methods

We extend a model developed by Qi *et al.* (18) that considers interacting populations of receptors and ligands contained in

Table 1. Legend of symbols in equations

Symbol	Quantity
F	Free energy
C_T	TCR concentration in T cell membrane
C_M	MHC-peptide concentration in supported membrane
C_{TM}	Concentration of TCR–MHC peptide complex
C_L	LFA-1 concentration in T cell membrane
C_I	ICAM-1 concentration in supported membrane
C_{LI}	Concentration of LFA-1–ICAM-1 complex
k_{on}	On rate for TCR–MHC-peptide binding
k_{off}	Off rate for TCR–MHC-peptide binding
k_{LI}	On rate for LFA-1–ICAM-1 binding
k_{-LI}	Off rate for LFA-1–ICAM-1 binding
D_j	Diffusion coefficient of the j th protein in the appropriate membrane
Z	Local intermembrane separation
z_j	Natural length of j th protein complex
t	Time
γ	Interfacial tension of cell membrane
κ	Bending rigidity of cell membrane
ζ	Thermal noise
$k_B T$	Thermal energy at temperature T
M	Phenomenological constant for membrane response to free-energy changes
λ_j	Curvature of binding energy well for j th protein complex
V	Speed of directed TCR transport

apposed membranes. One of the membranes (i.e., the cell membrane) is flexible and connected to a cytoskeletal complex. The other is flat and represents a supported bilayer. TCR and LFA-1 in the cell membrane can bind if apposed to the ligands MHCp and ICAM-1, respectively, in the supported bilayer. Receptor–ligand binding is characterized by on and off rates. Receptors and ligands are mobile in the two-dimensional planes of the membrane. Diffusion driven by concentration gradients or, in the case of TCR, a directed motion driven by cytoskeletal reorganization (32) determines mobility in the membrane. These processes of intramembrane protein motion and intermembrane receptor–ligand binding are described by Smoluchowski equations (Eqs. 1–6 below). The two pairs of receptors and ligands have different topographical sizes; the TCR–MHCp complex is $\approx 15 \text{ nm}$ in size, whereas the LFA-1–ICAM-1 complex is $\approx 40 \text{ nm}$ long (33–35). Thus, the rate of receptor–ligand binding depends on local intermembrane separation (k_{on} and k_{LI} are functions of z in Eqs. 1–6 below).

The intermembrane separation (or membrane shape) evolves in time according to Eq. 7 below, which is a time-dependent Landau–Ginzburg equation (36). This represents potential motion driving the membrane shape to that corresponding to the lowest free energy. Free-energy changes due to membrane-shape changes are influenced by three factors. Shape changes that result in creation of new area are penalized by an interfacial tension, and those that lead to the creation of high curvature manifolds are penalized by a bending rigidity (37). These effects are described by the third term in the free-energy functional in Eq. 8. The difference in receptor/ligand sizes influences the membrane free energy in one more way in the model. If a bonded receptor–ligand complex exists at a given location, then membrane-shape changes that deform the bond away from its natural length (e.g., 15 nm for TCR–MHCp and 40 nm for LFA-1–ICAM-1) lead to free-energy penalties that we model using a harmonic approximation (first two terms in Eq. 8). The difference in topographical size of the different receptor–ligand pairs and the fact that they are embedded in a cell membrane that cannot be deformed without incurring free-energy penalties provide a mechanism for sorting different receptors and ligands to separate regions of the membrane (16, 33, 38). Receptor mobility (directed or diffusive) is necessary for this sorting process.

The model developed by Qi *et al.* (18) includes TCR degradation in the simplest possible way (39–41). This effect is

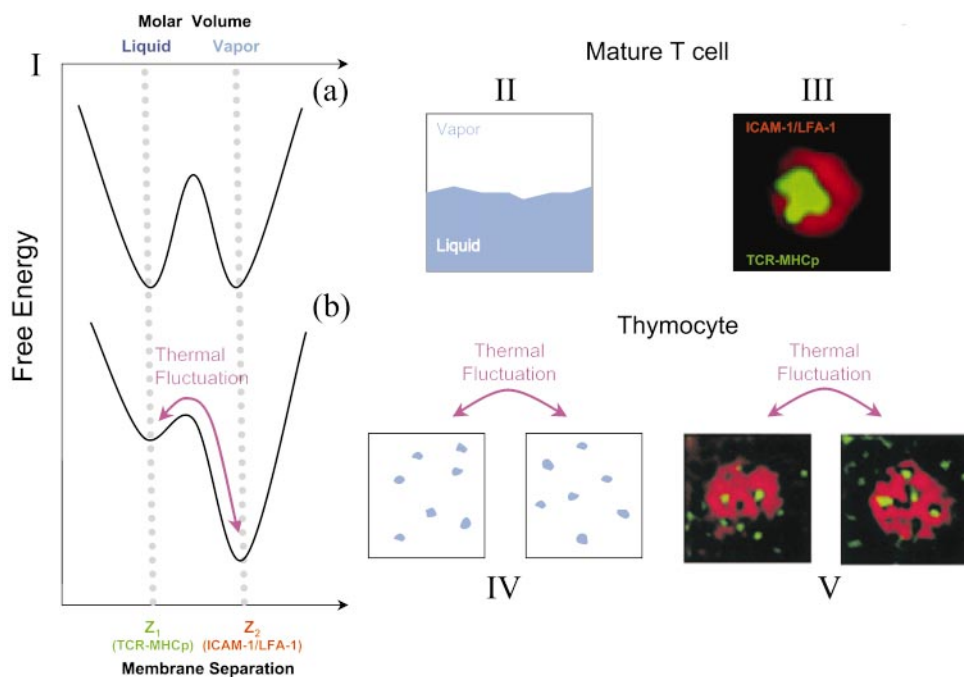


Fig. 2. (I) Free-energy profile as a function of intermembrane separation. The minimum at $z = 15$ nm corresponds to TCR–pMHC binding, and that at $z = 40$ nm corresponds to LFA-1–ICAM-1 binding. Curve a corresponds to a high TCR expression level, and curve b corresponds to a low TCR expression level. Analogous curves for the free-energy profile as a function of molar volume (density) for simple fluids at different temperatures. (II) Coexistence of liquid and vapor when free energy of vapor and liquid are comparable. (III) Coexistence of TCR–MHCp and LFA-1–ICAM-1 in the mature T cell synapse. (IV) Spatio-temporal density fluctuations of a simple fluid at temperatures above vapor–liquid coexistence. (V) Spatio-temporal concentration fluctuations of TCR–MHCp and LFA-1–ICAM-1 in dynamic multifocal synapses formed by thymocytes.

incorporated in Eq. 1 by the term P , which is proportional to $\exp[-k_{\text{off}}\tau]$. The following equations (symbols are defined in Table 1) embody a mathematical description of how receptor–ligand binding, protein mobility, and membrane-shape changes are inextricably linked during synapse formation.

$$\frac{\partial C_T}{\partial t} = D_T \nabla^2 C_T - k_{\text{on}}(z) C_T C_M + k_{\text{off}}(1 - P) C_{TM} - \vec{\nabla} \cdot (\vec{V} C_T) \quad [1]$$

$$\frac{\partial C_M}{\partial t} = D_M \nabla^2 C_M - k_{\text{on}}(z) C_T C_M + k_{\text{off}} C_{TM} \quad [2]$$

$$\frac{\partial C_{TM}}{\partial t} = D_{TM} \left[\nabla^2 C_{TM} + \frac{1}{k_B T} \vec{\nabla} \cdot \left(C_{TM} \vec{\nabla} \frac{\delta F}{\delta C_{TM}} \right) \right] + k_{\text{on}}(z) C_T C_M - k_{\text{off}} C_{TM} \quad [3]$$

$$\frac{\partial C_L}{\partial t} = D_L \nabla^2 C_L - k_{\text{LI}}(z) C_L C_I + k_{-\text{LI}} C_{LI} \quad [4]$$

$$\frac{\partial C_I}{\partial t} = D_I \nabla^2 C_I - k_{\text{LI}}(z) C_L C_I + k_{-\text{LI}} C_{LI} \quad [5]$$

$$\frac{\partial C_{LI}}{\partial t} = D_{LI} \left[\nabla^2 C_{LI} + \frac{1}{k_B T} \vec{\nabla} \cdot \left(C_{LI} \vec{\nabla} \frac{\delta F}{\delta C_{LI}} \right) \right] + k_{\text{LI}}(z) C_L C_I - k_{-\text{LI}} C_{LI} \quad [6]$$

$$\frac{\partial z}{\partial t} = -M \frac{\delta F}{\delta z} + \zeta \quad [7]$$

$$F = \frac{\lambda_{TM}}{2} \iint dxdy C_{TM}(x, y, t) [z(x, y, t) - z_1]^2 + \frac{\lambda_{LI}}{2} \iint dxdy C_{LI}(x, y, t) [z(x, y, t) - z_2]^2 + \frac{1}{2} \iint dxdy [\gamma (\nabla z)^2 + \kappa (\nabla^2 z)^2] \quad [8]$$

If we consider situations in which receptor–ligand binding/dissociation and protein mobility in the membrane are fast compared with membrane-shape changes during synapse formation, Eqs. 1–6 can be solved explicitly for the concentrations of the TCR–MHCp and LFA-1–ICAM-1 complexes. In particular, $C_{TM} \approx [k_{\text{on}}(z) C_T C_M] / k_{\text{off}}$ and $C_{LI} \approx [k_{\text{LI}}(z) C_L C_I] / k_{-\text{LI}}$. $k_{\text{on}}(z)$ and $k_{\text{LI}}(z)$ are Gaussians centered around 15 and 40 nm, respectively (18, 42). When these expressions are substituted into Eq. 8, the free-energy functional that controls the time evolution of intermembrane spacing (z) is one that has two minima centered around $z = 40$ and 15 nm. The depth of these free-energy minima depend on the propensity for LFA-1–ICAM-1 and TCR–MHCp binding, respectively. When receptor/ligand expression levels and binding constants are such that the two free-energy minima are comparably favorable and deeper than $k_B T$, thermal fluctuations in Eq. 7 are not important (Fig. 2I, curve a). This is the case for synapse formation in mature T cells, and a well organized synapse forms with TCR–MHCp coexisting with and segregated from LFA-1–ICAM-1 (5, 18). However, if TCR expression levels become smaller, the free-energy minimum corresponding to TCR–MHCp binding will become more shallow (Fig. 2I, curve b). For sufficiently small TCR expression, LFA-1–ICAM-1 will be dominant in the synapse and thermal fluctuations may become important. These random fluctuations provide a driving force for destroying order created by deterministic forces arising from receptor–ligand binding. In particular, they may result in short-lived TCR–MHCp clusters.

Because we wish to consider the effects of low TCR expression on synapse formation, in this article thermal fluctuations are considered explicitly. Thermal fluctuations represented by $\zeta(t)$ are drawn from a Gaussian distribution with 0 mean and variance determined by the fluctuation–dissipation theorem (37), i.e.,

$$\langle \zeta(r, t) \rangle = 0; \langle \zeta(r, t) \zeta(r', t') \rangle = 2Mk_B T \delta(r - r') \delta(t - t'),$$

where T is the temperature, k_B is Boltzmann's constant, r is the two-dimensional location in the intercellular junction, and δ represents the Dirac delta function. The parameters (details in Supporting Appendix, which is published as supporting information on the PNAS web site, www.pnas.org, and the figure legends) used to carry out the calculations reported in this article

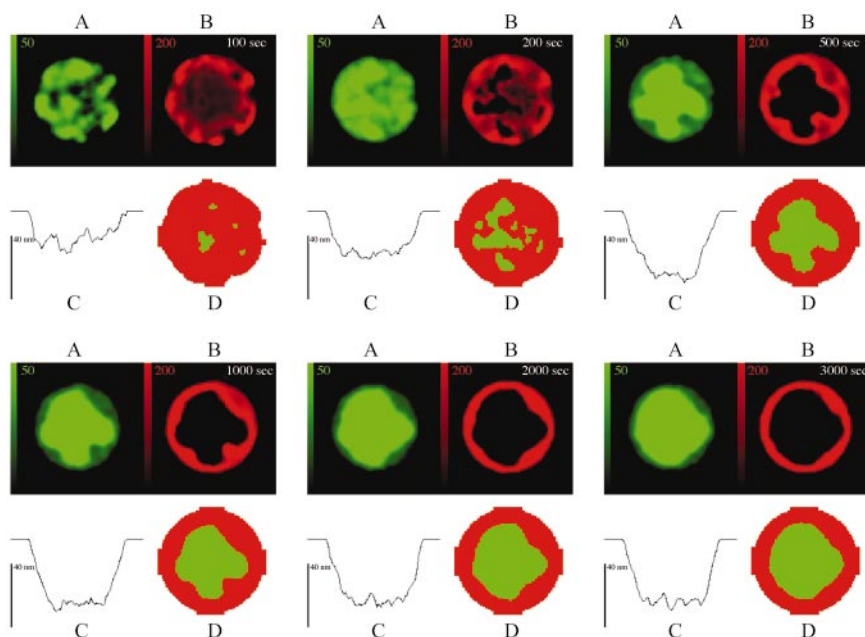


Fig. 3. Snapshots in time from a trajectory calculated by using our theoretical model for the peptide Hb64-76 ($k_{\text{on}} = 0.007 \mu\text{m}^2$ per molecule per s; $k_{\text{off}} = 0.064 \text{sec}^{-1}$). (A) Spatial distribution of MHCp (green). (B) Spatial distribution of ICAM-1 (red). (C) Side view of the cell-membrane shape at the center of the contact region. (D) Overlay of MHCp and ICAM-1 that is created by plotting the color green (red) when MHCp (ICAM-1) is the dominant species at a particular location. The TCR expression level is 200 molecules per μm^2 and corresponds to mature T cells (5, 18).

are the same as that used in previous studies that led to results similar to the experiments by Grakoui *et al.* (5).

Results

Fig. 3 shows results of our calculations in the case where TCR concentration is 200 molecules per μm^2 , the value used (18, 42) to model synapse formation between mature T cells and bilayer mimics of APCs (5). The TCR–MHCp binding kinetics correspond to Hb64-76 (5), the peptide used in the experiments by Hailman *et al.* (26). Values of other parameters are specified in *Supporting Appendix* and were used in earlier studies of synapse formation (18, 42). Snapshots of the distribution of ICAM-1 and MHCp at various time points are shown for a specific calculated trajectory (analogous to a particular experiment). In all such trajectories (see also Movies 1 and 2, which are published as supporting information on the

PNAS web site), we see that a mature synapse forms with the characteristic cSMAC and pSMAC in a few minutes.

Fig. 4 shows results of calculations for which all parameters in the model are kept the same as those corresponding to Fig. 3 except for the TCR concentration, which is lowered by 1 order of magnitude [consistent with experiments with thymocytes (26)]. Under these conditions, 75% of our calculated trajectories exhibit the behavior depicted in Fig. 4 (Movies 1 and 2). ICAM-1 is the dominant species in the intercellular junction. However, holes in the ICAM-1 structure correspond to MHCp clusters. These MHCp clusters appear in different regions of the synapse, evanesce, and then reappear in other parts of the junction. The behavior resembles the dynamic multifocal synapses observed in experiments (see Movies 1 and 2). These characteristics are observed below a threshold value of TCR expression. However,

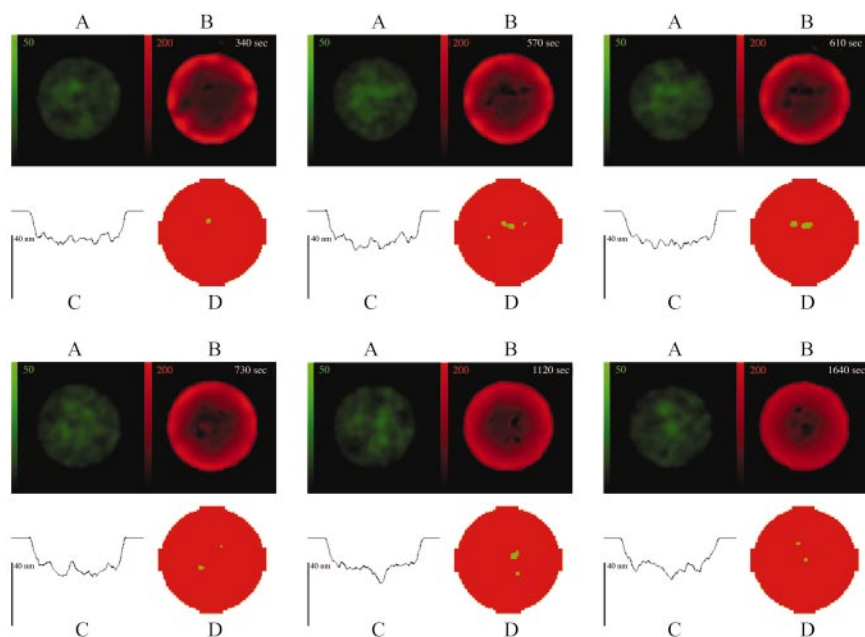


Fig. 4. Snapshots in time from a trajectory calculated by using our theoretical model for the peptide Hb64-76 ($k_{\text{on}} = 0.007 \mu\text{m}^2$ per molecule per sec; $k_{\text{off}} = 0.064 \text{sec}^{-1}$). (A) Spatial distribution of MHCp (green). (B) Spatial distribution of ICAM-1 (red). (C) Side view of the shape of the cell membrane shape at the center of the contact region. (D) Overlay of MHCp and ICAM-1 that is created by plotting the color green (red) when MHCp (ICAM-1) is the dominant species at a particular location. The TCR expression level is 1 order of magnitude smaller than that shown in Fig. 3 and corresponds to DP thymocytes (26).

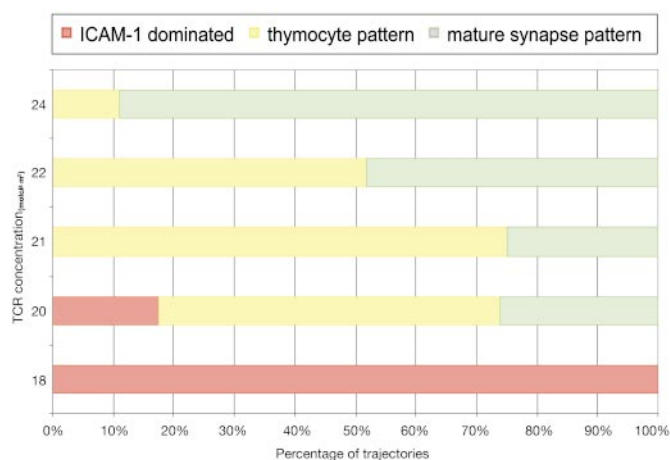


Fig. 5. Percentage of trajectories (analog of percentage of cells) that form synapses characteristic of mature T cells and thymocytes as a function of TCR expression level. As in recent experiments (26), as TCR expression level increases, the propensity for forming stable synapses characteristic of mature T cells increases. For very low levels of TCR, the synapse is dominated by ICAM-1 and does not contain MHCp clusters over long times.

below a certain even lower level of TCR expression, no MHCp clusters are observed in the synapse (Fig. 5).

We have carried out calculations with another MHCp characterized by the affinity of MCC88-103. The results (data not shown) are the same as that shown in Figs. 3 and 4. In other words, when TCR expression levels are ≈ 10 times smaller than that for mature T cells, dynamic multifocal synapses characteristic of thymocytes are observed. Thus, the formation of multifocal dynamic synapses for sufficiently small levels of TCR expression is not special for Hb64-76. We have also carried out calculations with and without allowing for TCR degradation (data not shown). In general, we find that the range of TCR expression levels corresponding to dynamic multifocal synapses is higher when TCR degradation is included.

Discussion

Receptor–ligand binding is energetically favorable. The difference in topographical size between the two types of receptor–ligand pairs implies that free-energy minima associated with TCR–MHCp binding and LFA-1–ICAM-1 binding correspond to different intermembrane separations (Fig. 2). TCR–MHCp binding propensity provides a force that favors an intermembrane separation of 15 nm, whereas LFA-1–ICAM-1 binding favors an intermembrane separation equal to 40 nm.

The depth of each minimum shown in Fig. 2 represents propensity for binding and is determined by the intrinsic molecular affinity and the concentrations of a receptor and its complementary ligand. This can be understood by using both kinetic and thermodynamic arguments. For example, if receptor–ligand binding is locally at equilibrium, then the concentration of the TCR–MHCp is given by $C_{TM} = (C_T C_M)/K_d$, where C_T and C_M are the local concentrations of unbound TCR and MHCp in the membranes, respectively. This expression shows that a larger TCR concentration leads to a larger concentration of bound TCR, which in turn implies that the free-energy minimum corresponding to intermembrane separation of 15 nm is deeper. This is because the larger the number of TCR–MHCp complexes, the greater the driving force to make the local intermembrane spacing equal 15 nm. The same point can be made by using the mass-action law, which states that the binding rate is $k_{on} C_T C_M$. Again, a larger pool of free TCR molecules corresponds to a greater rate, or driving force, for binding and an intermembrane separation of 15 nm. The same arguments apply to

LFA-1–ICAM-1 binding and the energy minimum at intermembrane separation equal to 40 nm.

Imagine that receptor concentration and ligand affinity for TCR and LFA-1 are such that the minima for intermembrane separations at 15 and 40 nm are roughly of the same depth. This is analogous to the free-energy profile as a function of density for a simple fluid (say, water) at temperatures that result in coexistence of liquid and vapor in separate regions of the same enclosure. Because of gravity, liquid occupies the lower part of the enclosure (see Fig. 2). Analogous to this situation, for TCR concentrations that result in mature T cell synapses, TCR–MHCp and LFA-1–ICAM-1 coexist in separate parts of the intercellular junction. The membrane-bending rigidity and tension play the role of gravity in this case, and a synapse with the shorter TCR–MHCp pair in the middle and the LFA-1–ICAM-1 pair in the periphery results because such a shape leads to a lower bending and interfacial free energy for the membrane.

When TCR concentration is lowered (as in thymocytes) compared with the situation described above, the driving force for TCR–MHCp binding is smaller, and the corresponding free-energy minimum (at 15 nm) is more shallow than that for LFA-1–ICAM-1 binding (at 40 nm). Now the free-energy profile (Fig. 2*I*, curve b) favors LFA-1–ICAM-1 binding, and in the absence of thermal fluctuations Fig. 4 would be red in color. However, thermally induced membrane-shape fluctuations will allow TCR–MHCp binding, and the corresponding free-energy minimum will be sampled sometimes. This minimum being more shallow, thermal fluctuations will also drive the system back to the red minimum more easily. In other words, the life time of this state is small compared with the life time of the red state. Thus, green spots will appear, live for a certain time that grows with the depth of the minimum, and then will evanesce. They then will reappear in other locations driven by thermal fluctuations. Such dynamic multifocal synapse formation is analogous to the formation of transient liquid droplets due to thermal density fluctuations in a fluid at temperatures above the boiling point (Fig. 2). For synapse formation, TCR expression level plays a role analogous to temperature for the behavior of a fluid.

The MHCp clusters observed in thymocyte synapses are $\approx 1 \mu\text{m}$ in size (E. Hailman, private communication). Typical sizes of liquid domains created by thermal fluctuations in a vapor phase are much smaller and get large only in the vicinity of the critical point. This difference between the analogous situations is primarily due to two reasons that result in a lower barrier between the two relevant free-energy minima (Fig. 2) for cell–cell interactions. In fluids, the widths of the free-energy minima corresponding to vapor and liquid are directly related to compressibilities of fluid phases, which are quite small. In contrast, the widths of the free-energy minima associated with binding of receptors and ligands embedded in membranes are determined by two factors. In addition to the analog of compressibility (i.e., the parameter λ_i , which measures bond flexibility), flexibility of receptor tethering to the cell membrane plays an important role in determining the range of intermembrane separations over which receptor–ligand binding can occur. The additional dependence of receptor–ligand binding propensity on z increases the widths of the free-energy minima which, in turn, lowers the effective barrier between the two minima. A second reason for the barrier being lower for cell–cell interactions is the lower dimensionality (equal to 2) compared with a fluid in a three-dimensional container. Thus, the intrinsic barrier height scales with MHCp cluster size less strongly than the barrier scales with droplet size in fluids. These factors, in a sense, make our system closer to a critical point in fluid systems where large droplets of liquid in a vapor are common. We do not observe clusters smaller than $1 \mu\text{m}$ with high probability in thymocyte synapses, because the membrane-bending energy strongly penalizes membrane deformations on length scales shorter than $\sqrt{\kappa/\gamma}$.

Fig. 5 shows that as the TCR expression increases from a value corresponding to situations in which multifocal dynamic synapses are observed, the likelihood of forming classical synapses characteristic of mature T cells becomes larger. This is because the free-energy minimum corresponding to TCR–MHCp binding becomes deeper (more favorable). This may be the reason why Hailman *et al.* found that a larger fraction of single-positive thymocytes [which have a higher TCR expression (43)] form classical synapses compared with DP thymocytes (26). We only observe dynamic multifocal synapses over a range of TCR concentrations (Fig. 5) because below a threshold level of TCR expression the life time of TCR–MHCp becomes unobservably small. The range of TCR expression level over which our model predicts formation of dynamic multifocal synapses is higher when TCR degradation is incorporated, because during the course of synapse formation the TCR concentration is lowered below the initial level of expression.

TCR expression levels are down-regulated at the DP stage by posttranscriptional mechanisms involving the molecule SLAP (29–

31). Our result that lower TCR expression in DP thymocytes leads to a synapse pattern different from that observed during mature T cell activation, which could lead to differential signaling, implies that down-regulation of TCR expression at the DP stage is not coincidental. Differential signaling mediated by a different synapse pattern when DP thymocytes interact with ligands in the thymus may be necessary to trigger thymocyte selection by using the same signaling molecules as those involved in mature T cell activation. The active form of the tyrosine kinase, Lck, is found to be maintained at high levels for a significantly longer period in thymocyte synapses (26, 27) compared with mature T cells (8, 13). Could this difference in the activity of membrane proximal signaling molecules be due to the different synapse patterns? Understanding these issues requires incorporating a model for signal transduction into the statistical mechanical model for synapse formation that we have studied here.

We thank S. Raychaudhuri, E. Robey, and E. Hailman for discussions. This work was supported by the National Institutes of Health.

1. Abbas, A. K., Lichtman, A. H. & Pober, J. S. (2000) *Cellular and Molecular Immunology* (Saunders, Philadelphia).
2. Harding, C. V. & Unanue, E. R. (1990) *Nature* **346**, 574–576.
3. Jenkins, M. K., Khoruts, A., Ingulli, E., Mueller, D. L., McSorley, S. J., Reinhardt, R. L., Itano, A. & Pape, K. A. (2001) *Annu. Rev. Immunol.* **19**, 23–45.
4. Martz, E., Parker, W. L., Gately, M. K. & Tsoukas, C. D. (1982) *Adv. Exp. Med. Biol.* **146**, 121–147.
5. Grakoui, A., Bromley, S. K., Sumen, C., Davis, M. M., Shaw, A. S., Allen, P. M. & Dustin, M. L. (1999) *Science* **285**, 221–227.
6. Monks, C. R., Freiberg, B. A., Kupfer, H., Sciaky, N. & Kupfer, A. (1998) *Nature* **395**, 82–86.
7. Krummel, M. F., Sjaastad, M. D., Wulfiging, C. & Davis, M. M. (2000) *Science* **289**, 1349–1352.
8. Lee, K. H., Holdorf, A. D., Dustin, M. L., Chan, A. C., Allen, P. M. & Shaw, A. S. (2002) *Science* **295**, 1539–1542.
9. Wulfiging, C., Sumen, C., Sjaastad, M. D., Wu, L. C., Dustin, M. L. & Davis, M. M. (2002) *Nat. Immunol.* **3**, 42–47.
10. Reichert, P., Reinhardt, R. L., Ingulli, E. & Jenkins, M. K. (2001) *J. Immunol.* **166**, 4278–4281.
11. Stoll, S., Delon, J., Brotz, T. M. & Germain, R. N. (2002) *Science* **296**, 1873–1876.
12. McGavern, D. B., Christen, U. & Oldstone, M. B. (2002) *Nat. Immunol.* **3**, 918–925.
13. Freiberg, B. A., Kupfer, H., Maslanik, W., Delli, J., Kappler, J., Zaller, D. M. & Kupfer, A. (2002) *Nat. Immunol.* **3**, 911–917.
14. Delon, J. & Germain, R. N. (2000) *Curr. Biol.* **10**, R923–R933.
15. Davis, D. M. (2002) *Trends Immunol.* **23**, 356–363.
16. Chakraborty, A. K. (2002) *Sci. STKE* **2002**, PE10–PE16.
17. van der Merwe, P. A. (2002) *Curr. Opin. Immunol.* **14**, 293–298.
18. Qi, S. Y., Groves, J. T. & Chakraborty, A. K. (2001) *Proc. Natl. Acad. Sci. USA* **98**, 6548–6553.
19. Bromley, S. K., Burack, W. R., Johnson, K. G., Somersalo, K., Sims, T. N., Sumen, C., Davis, M. M., Shaw, A. S., Allen, P. M. & Dustin, M. L. (2001) *Annu. Rev. Immunol.* **19**, 375–396.
20. Hogquist, K. A. (2001) *Curr. Opin. Immunol.* **13**, 225–231.
21. Goldrath, A. W. & Bevan, M. J. (1999) *Nature* **402**, 255–262.
22. Sebzda, E., Mariathasan, S., Ohteki, T., Jones, R., Bachmann, M. F. & Ohashi, P. S. (1999) *Annu. Rev. Immunol.* **17**, 829–874.
23. Ashton-Rickardt, P. G., Bandeira, A., Delaney, J. R., Van Kaer, L., Pircher, H. P., Zinkernagel, R. M. & Tonegawa, S. (1994) *Cell* **76**, 651–663.
24. Janeway, C., Rudensky, S., Rath, S. & Murphy, D. (1992) *Curr. Biol.* **2**, 26–28.
25. Sun, Z., Arendt, C. W., Ellmeier, W., Schaeffer, E. M., Sunshine, M. J., Gandhi, L., Annes, J., Petrzilka, D., Kupfer, A., Schwartzberg, P. L. & Littman, D. R. (2000) *Nature* **404**, 402–407.
26. Hailman, E., Burack, W. R., Shaw, A. S., Dustin, M. L. & Allen, P. M. (2002) *Immunity* **16**, 839–848.
27. Richie, L. I., Ebert, P. J., Wu, L. C., Krummel, M. F., Owen, J. J. & Davis, M. M. (2002) *Immunity* **16**, 595–606.
28. Bousso, P., Bhakta, N. R., Lewis, R. S. & Robey, E. (2002) *Science* **296**, 1876–1880.
29. Sosinowski, T., Pandey, A., Dixit, V. M. & Weiss, A. (2000) *J. Exp. Med.* **191**, 463–474.
30. Bonifacio, J. S., McCarthy, S. A., Maguire, J. E., Nakayama, T., Singer, D. S., Klausner, R. D. & Singer, A. (1990) *Nature* **344**, 247–251.
31. Maguire, J. E., McCarthy, S. A., Singer, A. & Singer, D. S. (1990) *FASEB J.* **4**, 3131–3134.
32. Wulfiging, C. & Davis, M. M. (1998) *Science* **282**, 2266–2269.
33. Dustin, M. L. & Shaw, A. S. (1999) *Science* **283**, 649–650.
34. Garboczi, D. N., Ghosh, P., Utz, U., Fan, Q. R., Biddison, W. E. & Wiley, D. C. (1996) *Nature* **384**, 134–141.
35. Garcia, K. C., Degano, M., Stanfield, R. L., Brunmark, A., Jackson, M. R., Peterson, P. A., Teyton, L. & Wilson, I. A. (1996) *Science* **274**, 209–219.
36. Hohenberg, P. C. & Halperin, B. I. (1977) *Rev. Mod. Phys.* **49**, 435–479.
37. Chaikin, P. M. & Lubensky, T. C. (2000) *Principles of Condensed Matter Physics* (Cambridge Univ. Press, Cambridge, U.K.).
38. Hori, Y., Raychaudhuri, S. & Chakraborty, A. K. (2002) *J. Chem. Phys.* **117**, 9491–9501.
39. Wofsy, C., Coombs, D. & Goldstein, B. (2001) *Biophys. J.* **80**, 606–612.
40. Valitutti, S., Muller, S., Cella, M., Padovan, E. & Lanzavecchia, A. (1995) *Nature* **375**, 148–151.
41. Itoh, Y., Hemmer, B., Martin, R. & Germain, R. N. (1999) *J. Immunol.* **162**, 2073–2080.
42. Lee, S. J. E., Hori, Y., Groves, J. T., Dustin, M. L. & Chakraborty, A. K. (2002) *Trends Immunol.* **23**, 492–499.
43. Shortman, K., Vremec, D. & Egerton, M. (1991) *J. Exp. Med.* **173**, 323–332.